Article

Discovery Medicine 2025; 37(202): 2812–2826
https://doi.org/10.24976/Discov.Med.202537202.234

Hydrogen Sulfide Promotes Angiogenesis and Is Associated With Sonic Hedgehog Signaling Pathway Activation After Focal Cerebral Ischemia in Rats

Haiyan Chen[1,2,3,†], Bingbing Qin[2,†], Pin Zheng[4], Guixin Yang[2], Ting Wu[2], Jie Wang[5], Jianmin Huang[2,*], Xuebin Li[1,2,3,6,*]

[1]Department of Neurology, The First Clinical Medical College of Jinan University, 510000 Guangzhou, Guangdong, China
[2]Department of Neurology, The Affiliated Hospital of Youjiang Medical University for Nationalities, 533000 Baise, Guangxi, China
[3]Key Laboratory of Research on Clinical Molecular Diagnosis for High Incidence Diseases in Western Guangxi of Guangxi Higher Education Institutions, 533000 Baise, Guangxi, China
[4]Department of Gastroenterology, The Affiliated Hospital of Youjiang Medical University for Nationalities, 533000 Baise, Guangxi, China
[5]Department of Nephrology, The Affiliated Hospital of Youjiang Medical University for Nationalities, 533000 Baise, Guangxi, China
[6]School of Clinical Medicine, Youjiang Medical University for Nationalities, 533000 Baise, Guangxi, China
*Correspondence: bshuangjianmin@126.com (Jianmin Huang); xuebinlillxb_d@126.com (Xuebin Li)
†These authors contributed equally.
Submitted: 24 July 2025 Revised: 11 September 2025 Accepted: 28 September 2025 Published: 20 November 2025

Background: Ischemic stroke remains a leading cause of disability and mortality worldwide, with limited therapeutic options beyond acute reperfusion. Promoting angiogenesis and collateral circulation in ischemic penumbra is crucial for neurological recovery, yet the underlying mechanisms are not fully understood. This study investigates the regulatory role of hydrogen sulfide (H_2S) in angiogenesis and its associated molecular mechanisms in ischemic penumbra following transient focal cerebral ischemia in rats, with particular focus on examining the potential involvement of the Sonic hedgehog (SHH) signaling pathway.

Methods: Focal cerebral ischemia was induced via middle cerebral artery occlusion, with 90-minute reperfusion, in Sprague–Dawley rats. The rats were grouped as sham-7d, sham-14d, model-7d, model-14d, morpholin-4-ium 4-methoxyphenyl(morpholino) phosphinodithioate (GYY4137)-7d, and GYY4137-14d, according to the treatment method and length of observation. Neurofunctional assessments included Longa scale and beam walking tests. Plasma H_2S levels, cerebral blood flow, infarct volume, microvessel density, and expression of relevant proteins were measured using microassay, laser speckle imaging, 2,3,5-triphenyltetrazolium chloride (TTC) staining, Ki67/CD31 co-immunofluorescence, double immunofluorescence, and Western blotting, respectively.

Results: In GYY4137-treated rats, neurobehavioral performance improved significantly and plasma H_2S levels also significantly increased, compared to those of the model group ($p < 0.05$). Furthermore, cerebral blood flow showed substantial recovery, infarct volumes were significantly reduced, and microvessel density was augmented ($p < 0.05$). Immunofluorescence analysis revealed colocalization of vascular endothelial growth factor (VEGF), fibroblast growth factor 2 (FGF2), and angiopoietin 1 (ANG1) with CD31-positive endothelial cells. Western blot analysis demonstrated that ANG1, FGF2, VEGF, and SHH proteins were upregulated while cystathionine-β-synthase was downregulated in response to GYY4137 treatment ($p < 0.05$).

Conclusion: H_2S upregulates the expression of VEGF, ANG1, and FGF2 proteins in the peri-infarct tissue of rats, accompanied by activation of the SHH signaling pathway, promoting angiogenesis and collateral circulation, thereby significantly improving neurological function. These findings suggest that the SHH signaling pathway may be involved in H_2S-mediated pro-angiogenic effects, although further mechanistic validation is warranted.

Keywords: hydrogen sulfide; sonic hedgehog; angiogenesis; collateral circulation; neurological function; ischemic stroke

Introduction

Cerebral infarction is typically ensued by the induction of angiogenesis, which leads to the formation of tertiary cerebral collateral circulation. The establishment of cerebral collateral circulation has been shown to facilitate neurological functional recovery, enhance neural repair processes, and improve clinical prognosis in cerebral infarction [1–4]. However, the regulatory mechanisms underlying collateral circulation formation post-infarction are incompletely understood. Hydrogen sulfide (H_2S) is the third endogenous gaseous signaling molecule discovered in humans, after nitric oxide and carbon monoxide; it has a spectrum of physiological functions, such as neuroprotective, anti-inflammatory, and antioxidant properties [5]. Most research on H_2S's impact on angiogenesis has concentrated on its anti-angiogenic effects in cancer therapy and its angiogenesis-promoting roles in ischemic diseases, notably those affecting the myocardium [6]. However, its potential role in fostering collateral circulation development following cerebral infarction remains inadequately explored. The Sonic hedgehog (SHH) signaling pathway consists of the SHH protein and its downstream factors, including the receptor fragment protein Patched, the G-protein-coupled receptor Smoothened, and the glioma-associated oncogene homolog Glioblastoma factors. This pathway plays a crucial regulatory role in neural development and repair processes [7,8].

Accumulating research findings have revealed that the SHH signaling pathway participates in the regulation of angiogenesis through various mechanisms, including modulating the activity of multiple biomolecules and signaling pathways. For instance, SHH indirectly promotes angiogenesis by inducing fibroblasts to release vascular endothelial growth factor (VEGF) and fibroblast growth factor 2 (FGF2), as well as regulating the expression of angiopoietins such as angiopoietin 1 (ANG1) and angiopoietin 2 (ANG2) [9,10]. Additionally, stimulation of the SHH signaling pathway enhances the stability of vascular endothelial cells and the complex morphogenesis of vascular morphology by continuously inducing the activity of the Notch signaling pathway, thereby promoting vasculogenesis [11]. Several studies have explored the roles of H_2S and the SHH signaling pathway in cancer cells and certain disease models. These studies indicate a correlation between the activity of H_2S, the activity of H_2S synthase, and the activation of the SHH signaling pathway [12]. Additionally, there is a relationship between the overexpression of SHH protein and the expression of H_2S-producing enzymes [13]. To administer H_2S in a controlled and therapeutically relevant manner, morpholin-4-ium 4-methoxyphenyl(morpholino) phosphinodithioate (GYY4137)—a water-soluble, slow-releasing H_2S donor—has been developed. Unlike rapid H_2S donors such as sodium hydrosulfide (NaHS), which cause immediate but transient H_2S release, GYY4137 provides sustained and controlled H_2S release over extended periods, more closely mimicking physiological H_2S production patterns while reducing potential toxicity associated with sudden high concentrations.

Based on these findings, we hypothesized that H_2S and the SHH signaling pathway play pivotal roles in the establishment of collateral circulation after cerebral infarction and may exhibit a certain degree of interplay. Therefore, this study aimed to investigate the effects of H_2S on angiogenesis following cerebral infarction and examine the potential association with the SHH signaling pathway activation.

Materials and Methods

Animals and Experimental Design

This study employed 108 healthy adult male Sprague–Dawley rats that were of SPF-grade and weighed 230–260 g each; they were commercially sourced from Guangdong Vital River Laboratory Animal Technology Co., Ltd. (Production License No. SCXK (Yue) 2022-0063, Animal Quality Certificate No. 4482970021355). All experimental procedures were conducted in strict adherence to the "3R principles" (Replacement, Reduction, and Refinement) and the Guidelines for the Care and Use of Laboratory Animals published by the National Institutes of Health. The study was approved by the Ethics Committee of Youjiang Medical University for Nationalities (Approval No. 2023102701). Prior to the experiment, all the rats were acclimatized to the standardized housing conditions for one week. Environmental parameters were maintained as follows: ambient temperature 24 ± 2 °C, relative humidity 60 ± 5%, and automated 12-hour light/dark cycles. Standard laboratory chow and sterile drinking water were provided ad libitum. Husbandry practices included routine cage bedding replacement every 2–3 days to ensure optimal animal welfare standards. Following acclimatization, the rats were randomly stratified into six distinct experimental groups (n = 18 per group): a sham-operated control group with 7-day observation (sham-7d), sham-operated control group with 14-day observation (sham-14d), middle cerebral artery occlusion/reperfusion (MCAO/R) model group with 7-day observation (model-7d), MCAO/R model group with 14-day observation (model-14d), GYY4137-treated MCAO/R intervention group with 7-day observation (GYY4137-7d), and GYY4137-treated MCAO/R intervention group with 14-day observation (GYY4137-14d). GYY4137 was purchased from MCE (HY-107632-1g; Shanghai, China). Randomization was performed using a computer-generated sequence to ensure unbiased distribution across treatment groups. Six rats from each group were randomly selected for laser speckle imaging to monitor cerebral blood flow (CBF) and 2,3,5-triphenyltetrazolium chloride (TTC) staining, six for immunofluorescence detection after heart perfusion, and six for Western blot analysis.

MCAO/R Model Creation

The rats were anesthetized with isoflurane gas using a small animal anesthesia machine. A high-speed microdrill was used to uniformly thin the right parietal bone while maintaining the integrity of the dura mater, creating a rectangular cranial window extending from the bregma anteriorly to the coronal suture posteriorly, and from the sagittal suture medially to the lateral temporal line laterally [14]. Following cranial window preparation, the MCAO/R model was established [15] by advancing a 0.33 mm diameter filament with a blunt distal end into the lumen of the right middle cerebral artery (MCA) to a predetermined depth of 18 ± 2 mm. After maintaining vascular occlusion for 1.5 hours, reperfusion was initiated by carefully retracting the filament. The sham-operated rats underwent identical surgical procedures, except for the filament insertion. Following successful resuscitation, the rats were evaluated using the Longa neurobehavioral scoring system [15]; those scoring between 1 and 3 points were included in the experimental cohorts. Rats in the GYY4137 therapeutic cohorts were administered with daily intraperitoneal injections of 20 mg/kg H_2S controlled-release compound GYY4137. Both control cohorts (the sham-operated and ischemic model groups) received equivalent volumes of vehicle solution (DMSO + physiological saline) via the same intraperitoneal injection protocols. This standardized intervention protocol was applied in two distinct regimens: 7-day and 14-day periods, with all administrations performed once daily.

Monitoring of CBF Changes via Laser Speckle Imaging

Rats were placed under the microscope of the laser speckle imaging system and the focal length was adjusted to clearly visualize the cortical vessels in the MCA territory of the right hemisphere. A rectangular region of interest was selected within the right cerebral hemisphere of each rat, and CBF was recorded within this region. The size and location of the region of interest were consistent across all the rats. CBF was recorded at the following time points: pre-modeling; 1.5 hours post-MCA occlusion (MCAO); and 1-, 7-, and 14-day post-reperfusion. Thirty CBF images were acquired at each time point. Data analysis was conducted using RFLSI laser speckle analysis software (RWD Life Science, Shenzhen, China).

Assessment of Neurological Function

Body weights were measured daily using a digital scale (Model Scout Pro, Shanghai, China; accuracy ±0.1 g) from pre-modeling through 7- or 14-day post-reperfusion. At the 7th and 14th days post-surgery, neurological function was assessed using the Longa scoring system [15]. The scoring system is defined as follows: '0' represents normal limb motor function; '1' indicates partial impairment in the affected forelimb with failure to fully extend; '2' indicates spontaneous circling towards the paretic side during locomotion; '3' represents loss of balance with lateral falls to the affected side during ambulation; and '4' indicates complete inability to ambulate independently, accompanied by consciousness disturbances. For the beam walking test [16], a score of '0' was given if the rat could jump onto the beam and walk freely without falling, '1' if the rat could jump onto the beam but fell off with a probability of less than 50%, '2' if the rat could jump onto the beam but fell off with a probability greater than 50%, '3' if the rat could jump onto the beam but dragged its paralyzed hindlimb, and '4' if the rat could not jump onto the beam at all.

Collection and Examination of Peripheral Blood Samples

Prior to modeling, and 7- and 14-day post-ischemia-reperfusion, 1 mL of blood sample was collected from each rat under anesthesia by orbital bleeding [17] into EDTA-containing tubes. After a 20-minute incubation period at ambient temperature, the samples were centrifuged at 3500 rpm and 4 °C for 10 minutes. The plasma was separated and aliquoted into EP tubes for subsequent detection of H_2S in the peripheral blood. All components of the H_2S kit (Catalog # ml076943, Mlbio Biotechnology, China), including standards and plasma samples, were brought to room temperature before use. The assay was performed according to the manufacturer's instructions. The ΔA value (Ameasured – Ablank) was calculated for each well and then substituted into the following formula to calculate the H_2S concentration.

$$H_2S\ (\text{nmol/mL}) = \Delta A/0.0022 \times V_{\text{total reaction}} \div V_{\text{sample}} = 681.8 \times \Delta A$$

where $V_{\text{total reaction}}$ denotes the entire reaction volume, and V_{sample} indicates the specific volume of the biological specimen incorporated into the reaction mixture.

TTC Staining and Calculation of Cerebral Infarct Volume

Immediately post-euthanasia, the animal's brain was carefully harvested and rapidly frozen in a –80 °C freezer for 10 minutes to achieve controlled tissue hardening prior to coronal sectioning. Five 2 mm coronal sections were prepared and immersed in 2% TTC staining solution (Catalog # DK0005, Reagan Biology, China), protected from light exposure by aluminum foil wrapping, and then incubated at 37 °C for 20 minutes with intermittent agitation. Upon completion of staining, the sections were fixed in 10% neutral buffered formalin and digitally imaged for subsequent analysis of cerebral infarct volume.

Double Immunofluorescence Staining

Rats were euthanized via an overdose of isoflurane (5% in oxygen) anesthesia, in compliance with the NIH guidelines, for immunofluorescence studies. At the designated time point, the brain specimens were perfused and fixed with saline and paraformaldehyde, followed by coronal frozen sectioning. The sampling site was the cortical tissue surrounding the infarction at the striatal level, with a slice thickness of 12 μm. Following phosphate-buffered saline (PBS) rinsing, the tissue sections were subjected to antigen retrieval using citrate buffer prior to blocking in a solution containing 0.5% Triton X-100, 5% goat serum, and PBS. Diluted solutions of primary antibodies, as indicated in the following, were applied: rabbit anti-CD31 monoclonal antibody (Ab281583, Lot # GR789012, Abcam; 1:50), rat anti-Ki67 monoclonal antibody (14-5698-80, Lot # 135467, Invitrogen; 1:200), mouse anti-VEGF monoclonal antibody (MA1-16629, Lot

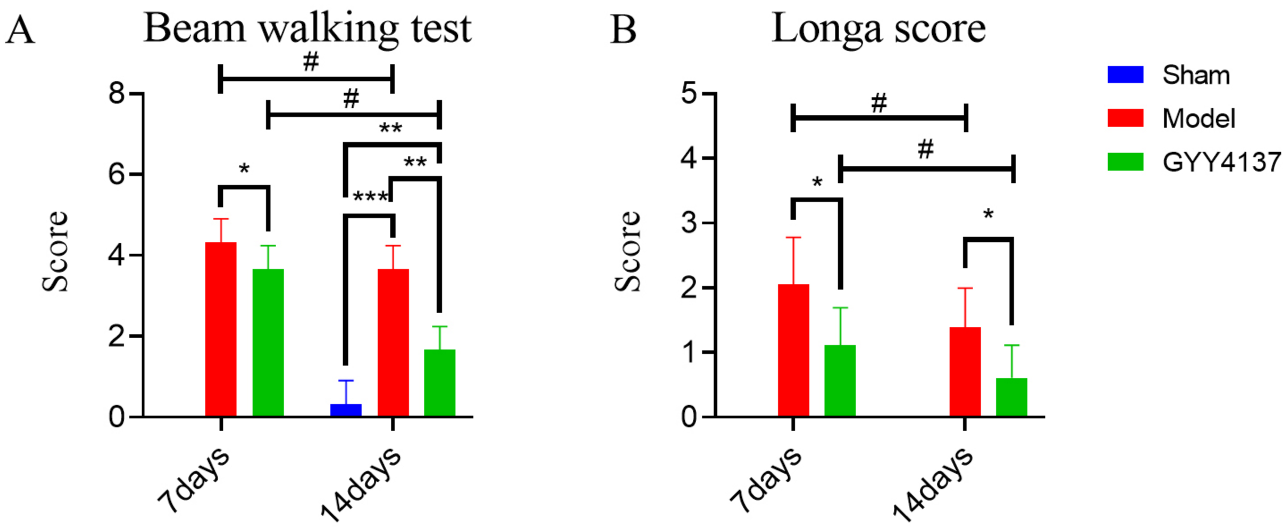

Fig. 1. Morpholin-4-ium 4-methoxyphenyl(morpholino) phosphinodithioate (GYY4137) treatment improves neurological function in middle cerebral artery occlusion/reperfusion (MCAO/R) rats at 7-and 14-day post-reperfusion. (A) Comparison of beam walking test scores among rats in different cohorts. (B) Comparison of Longa scores among rats in different cohorts. Notes: $^{*}p < 0.05$, $^{**}p < 0.01$, $^{***}p < 0.001$, $^{\#}p < 0.05$; each group consisted of 18 rats (n = 18).

254893, Invitrogen; 1:200), mouse anti-ANG1 monospecific antibody (sc-74528, Lot # GR890123, Santa Cruz; 1:50), and mouse anti-FGF2 monoclonal antibody (Lot # 554890, Boster; 1:100). The tissue sections were allowed to react with the primary antibodies for an 18-hour incubation period at 4 °C. After rinsing with PBS, appropriate fluorescent-labeled secondary antibodies were applied to the specimens. The following secondary antibody concentrations were employed: Alexa Fluor™ 594-conjugated caprine anti-rabbit immunoglobulin G (H+L) with extensive cross-absorption (Lot # 48963212, Invitrogen; 1:500), AF488-labeled caprine anti-rat immunoglobulin G (H&L) (Ab150157, Lot # 426012, Abcam; 1:500), and AF488-tagged caprine anti-mouse immunoglobulin G (H&L) (550047, Lot # 486334, Zen Bio; 1:500). The slices of tissue specimens were exposed to the secondary antibodies for 1 hour under light-protected conditions. Nuclear staining was achieved using DAPI. After staining and cover slipping, the specimens were examined and photographed using an epifluorescence microscope (Leica Microsystems, Wetzlar, Germany).

Determination of Microvessel Density

For each sample, six sections were examined, with two non-overlapping 40× fields selected from dorsal and ventral infarction-adjacent tissues per section. ImageJ 1.53e (NIH, USA) was used to determine the number of CD31 and KI67 double-positive endothelial cells, branch points, vessel lengths, and neovascular surface area.

Western Blotting

Rats were euthanized via an overdose of isoflurane (5% in oxygen), followed by decapitation for extracting brain specimens for use in Western blot analyses. Cortical tissue (weighing approximately 100 mg) of adjacent to the infarct region in the right cerebral hemisphere was dissected. Cerebral samples were disrupted and homogenized under refrigeration. Following centrifugation, the aqueous phase was collected, and the protein content was quantified via a bicinchoninic acid assay using Pierce BCA Protein Assay Kit (Catalog # ZJ102, Yamei Enzyme Scientific, China). The protein samples were electrophoresed using sodium dodecyl sulfate polyacrylamide gel electrophoresis (SDS-PAGE), and the separated protein bands were subsequently transferred to nitrocellulose membranes. The nitrocellulose membranes were subjected to blocking with non-fat milk for 2 hours, followed by 18-hour incubation at 4 °C with the following primary antibodies: rabbit anti-cystathionine-β-synthase (CBS) monoclonal antibody (ab313382, Abcam; 1:1000), rabbit anti-SHH monospecific antibody (347501, Zen Bio; 1:1000), rabbit anti-VEGF monoclonal antibody (Ab214424, Abcam; 1:1000), rabbit anti-FGF2 monospecific antibody (251703, Zen Bio; 1:1000), and rabbit anti-ANG1 monoclonal antibody (sc-74528, Santa Cruz; 1:1000). Afterwards, goat anti-rabbit IgG HRP-conjugated secondary antibody (511203, Zen Bio; 1:2000) was applied to the membranes, followed by a room-temperature incubation for 45 min. Chemiluminescent detection was performed using enhanced chemiluminescence substrate and a gel documentation system, with subsequent band intensity quantification via ImageJ software.

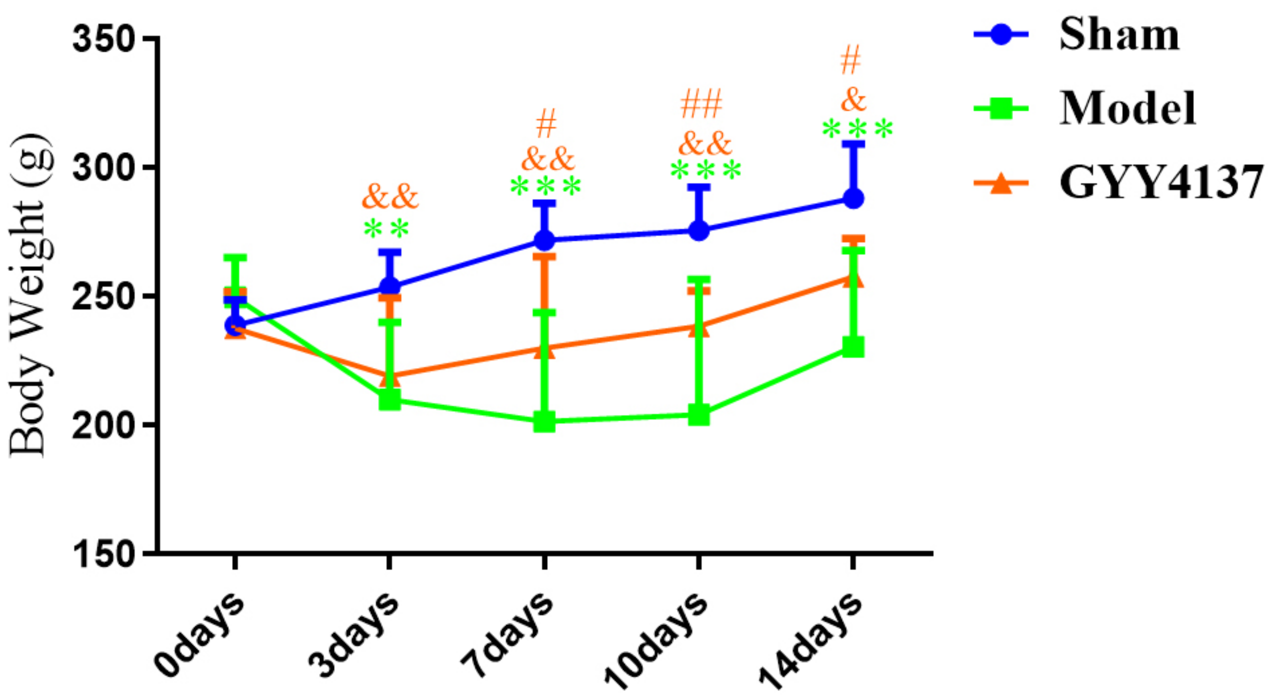

Fig. 2. H_2S donor GYY4137 recovered body weight in MCAO/R rats. Notes: "*" represents the model group comparison with the sham group, $^{**}p < 0.01$, $^{***}p < 0.001$; "&" represents the GYY4137-treated group comparison with the sham group, $^{\&}p < 0.05$, $^{\&\&}p < 0.01$, "#" represents the GYY4137-treated group comparison with the model group, $^{\#}p < 0.05$, $^{\#\#}p < 0.01$; each group consisted of 18 rats ($n = 18$).

Statistical Analysis

Quantitative data analysis and visualization were performed using GraphPad Prism 9.0 software (GraphPad Software, San Diego, CA, USA). Prior to statistical comparisons or analyses, normality of all data was assessed using the Kolmogorov–Smirnov test. Normally distributed data are expressed as mean ± standard deviation. Non-normal data were analyzed using the Mann–Whitney *U* test. For cross-sectional data at each time point, One-way analysis of variance (ANOVA) was used in multi-group comparisons, followed by Fisher's LSD post hoc test for pairwise evaluations. The Student's *t*-test was employed for within-group temporal comparisons and between-group comparisons at individual time points. For longitudinal data presented in line graphs (body weight, plasma H_2S levels, and cerebral blood flow), one-way ANOVA was performed at each individual time point to compare differences among the three groups (Sham, Model, and GYY4137), as measurements at different time points involved partially independent samples due to terminal tissue collection at 7-day and 14-day endpoints. Results with $p < 0.05$ were considered statistically significant.

Results

Effect of H_2S on MCAO/R Rats' Neurobehavioral Outcomes

Rats in the sham group exhibited no symptoms of neurological deficit, whereas rats in both the pathological model cohort and the GYY4137-treated cohort displayed varying degrees of neurological deficit. When compared with the model group at corresponding time points, rats in the GYY4137-treated group showed significantly lower scores in both the beam walking test and the Longa scoring evaluation ($p < 0.05$). Notably, longitudinal analysis revealed that the GYY4137-14d group showed significantly lower deficit scores compared to the GYY4137-7d ($p < 0.05$) (Fig. 1).

Effect of H_2S on Body Weight of MCAO/R Rats

Body weights were measured preoperatively and 3, 7, 10, and 14 days postoperatively. The rats had comparable body weights preoperatively ($p > 0.05$ for all comparisons). After surgery, the model and GYY4137-treated groups weighed less than the sham group did ($p < 0.05$), but the GYY4137-treated rats outperformed the model rats in achieving more significant body weight recovery at 7, 10, and 14 days post-operatively ($p < 0.05$) (Fig. 2).

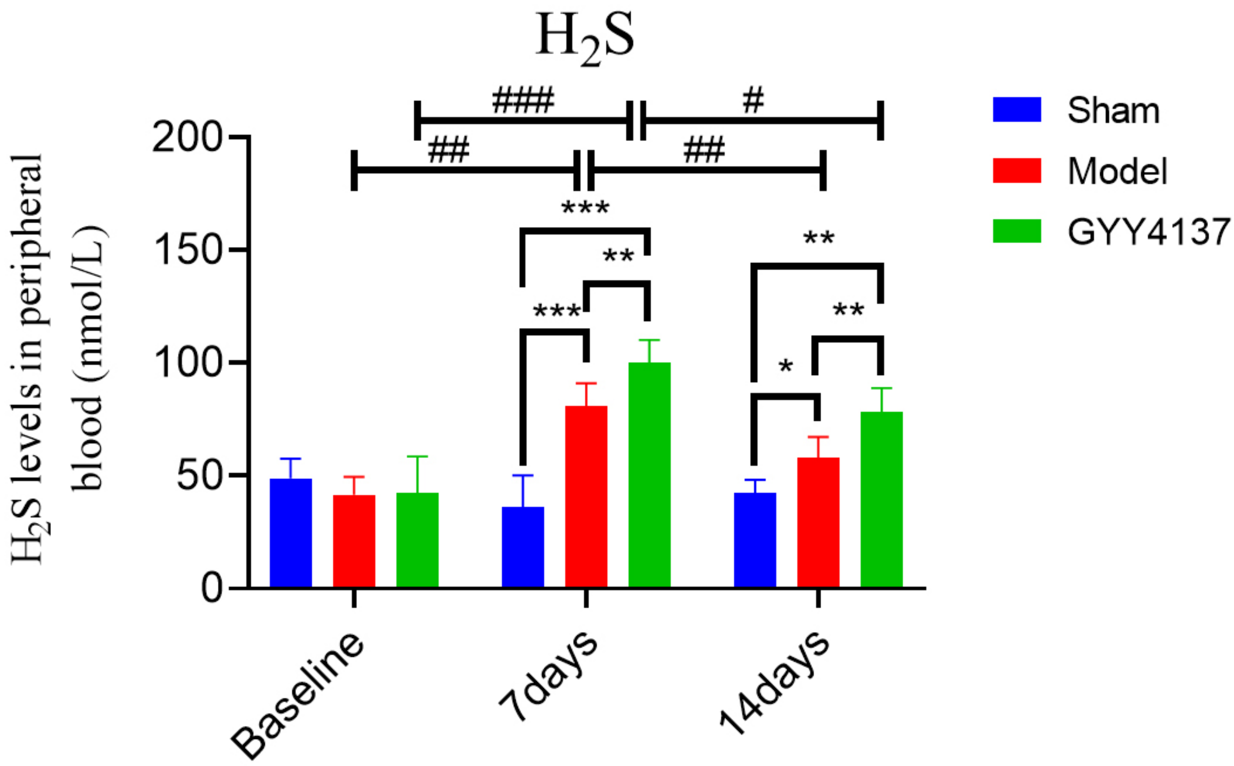

Fig. 3. GYY4137 enhances plasma H_2S levels in MCAO/R rats. Note: "*" represents comparison between groups, $^{*}p < 0.05$, $^{**}p < 0.01$, $^{***}p < 0.001$; "#" represents comparison within group, $^{\#}p < 0.05$, $^{\#\#}p < 0.01$, $^{\#\#\#}p < 0.001$; each group consisted of 18 rats (n = 18).

Comparison of Plasma H_2S Levels Among Different Groups

Our findings indicate that, relative to pre-modeling baseline measurements, plasma H_2S levels in the sham group exhibited no statistically significant difference across all sampled time intervals ($p > 0.05$). However, plasma H_2S levels in the model and GYY4137-treated groups were significantly elevated throughout the observation period ($p < 0.05$). Furthermore, as time progressed, the plasma H_2S levels declined ($p < 0.05$). Comparative assessment between the experimental groups showed that postoperative H_2S levels in the GYY4137-treated groups remained significantly higher than those in the model groups across all time points ($p < 0.05$) (Fig. 3).

Effects of H_2S on CBF in MCAO/R Rats

CBF in the right cerebral hemisphere of rats from each group was monitored at various time points using laser speckle imaging. Normal CBF perfusion was observed in the right cerebral hemisphere of rats across all groups preoperatively. However, following the induction of MCAO, CBF in the right cerebral hemisphere was significantly decreased at 1.5 hours post-occlusion, and remained low at 1-, 7-, and 14-day post-reperfusion in the model and GYY4137-treated cohorts ($p < 0.05$). Following reperfusion (removal of the intraluminal thread), CBF in the right cerebral hemisphere of rats in the model and GYY4137-treated cohorts showed varying degrees of recovery at different time points. Relative to the model cohort, the GYY4137-treated rats demonstrated marked restoration of CBF at 7 and 14 days postoperatively ($p < 0.05$) (Fig. 4).

Assessment of Cerebral Infarct Volume in MCAO/R Rats Using TTC Staining

TTC staining distinguishes infarcted brain tissue (appears white) from viable tissue (red), allowing quantification of infarct volume as the percentage of white area relative to total tissue area. The results showed that rats in the sham group exhibited no white infarct lesions, while those in the model and GYY4137-treated groups displayed white areas of varying sizes in the right cerebral hemisphere. Statistical analysis indicated no significant difference in the infarct volumes between the Model-7d and Model-14d groups ($p > 0.05$). Relative to the model group, both the GYY4137-7d and GYY4137-14d groups exhibited significant reductions in cerebral infarction volume ($p < 0.05$). Extended administration of GYY4137 over 14 days resulted in significantly smaller cerebral lesions compared to those observed in the group receiving 7-day treatment regimen ($p < 0.05$) (Fig. 5).

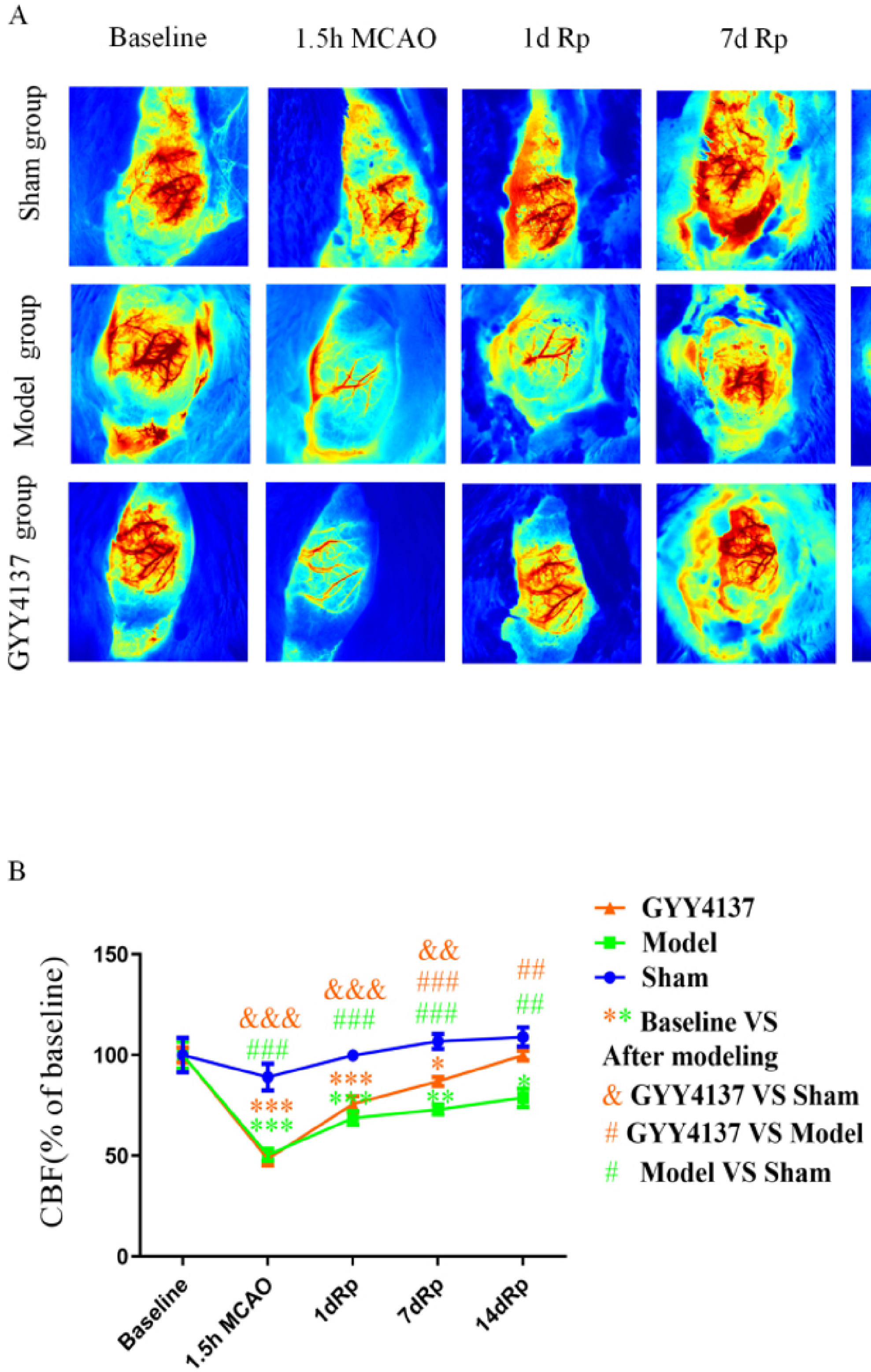

Fig. 4. GYY4137 restores cerebral blood flow (CBF) in the ischemic penumbra of MCAO/R rats. (A) Representative laser speckle images of CBF in the right hemisphere of a rat at baseline, 1.5 hours post-MCAO, and 1-, 7-, and 14-day post-reperfusion (indicated as 'Rp'). (B) Statistical plot of CBF percentage relative to baseline for each rat, presented as mean ± SD. Note: "*" represents comparison with the baseline, $^{*}p < 0.05$, $^{**}p < 0.01$, $^{***}p < 0.001$; "#" represents comparison with the model group, $^{\#\#}p < 0.01$, $^{\#\#\#}p < 0.001$; "&" represents comparison with the sham group, $^{\&\&}p < 0.01$, $^{\&\&\&}p < 0.001$; each group consisted of 12 rats (n = 12).

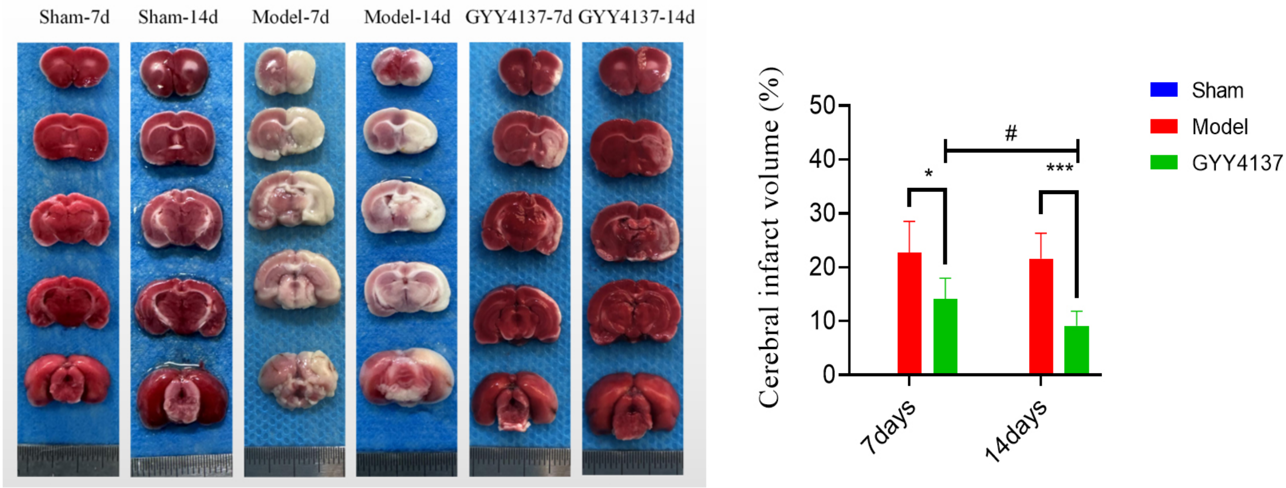

Fig. 5. GYY4137 reduces cerebral infarct volume in MCAO/R rats at 7- and 14- days post-operatively. Representative TTC-stained brain sections from per group are shown. Data from 6 rats were used for quantitative analysis per group. Notes: $^{*}p < 0.05$, $^{***}p < 0.001$; $^{\#}p < 0.05$.

Effects of H_2S on Microvessel Density in the Peri-Infarct Cortex of MCAO/R Rats

Ki67 and CD31 double-staining was used to assess microvessel density in the peri-infarct cortex of the rats by comparing the number of neovascular branch points, vessel length, surface area, and Ki67$^+$/CD31$^+$ double-positive cells. The results showed that the sham group had reduced number of neovascular branch points, vessel length, surface area, and number of Ki67$^+$/CD31$^+$ double-positive cells, with consistent expression levels at 7 and 14 days (all $p > 0.05$). The model group had elevated levels of these parameters relative to the sham group ($p < 0.05$), but specifically, the model-7d group demonstrated higher levels of these indicators compared to the model-14d group ($p < 0.05$). The levels of these indicators were further enhanced by GYY4137 treatment ($p < 0.05$). The GYY4137-treated group showed significant increases of these parameters compared to both the model-7d and model-14d groups ($p < 0.05$). Moreover, intra-regimen comparison analysis showed that the GYY4137-7d group had higher levels of these parameters than the GYY4137-14d group ($p < 0.05$) (Fig. 6).

H_2S Modulates ANG1, FGF2, and VEGF Expression in the Peri-Infarct Cortex of MCAO/R Rats

To investigate the underlying mechanisms of H_2S-mediated microvessel density in MCAO/R rats, we assessed ANG1, FGF2, and VEGF expression in the peri-infarct cortex of the rats via CD31 co-immunofluorescence. The results showed that ANG1, FGF2, and VEGF were expressed in the CD31$^+$ vascular endothelial cells of the peri-infarct tissues. Compared to the sham groups at the corresponding time points, the model groups exhibited significantly increased number of ANG1$^+$/CD31$^+$, FGF2$^+$/CD31$^+$, and VEGF$^+$/CD31$^+$ double-positive cells ($p < 0.05$). The rats of the model-7d group exhibited a higher number of these cells than their counterparts in the model-14d ($p < 0.05$). The GYY4137 intervention further enhanced the proportions of these double-positive cells, compared to those observed in the sham and model groups at corresponding time points ($p < 0.05$), with peak expression at day 7 (all $p < 0.05$) (Figs. 7,8,9). Western blot analysis further confirmed the protein expression profiles of ANG1, FGF2, and VEGF, which were consistent with the immunofluorescence findings (Fig. 10).

Effect of H_2S on the SHH Signaling Pathway

To elucidate the relationship between the endogenous H_2S production capacity and the exogenous H_2S therapeutic effects, we examined the expression of CBS alongside SHH signaling pathway activation in the peri-infarct cortical tissues of MCAO/R rats via Western blotting. CBS, as the primary H_2S-producing enzyme, serves as a biomarker for endogenous H_2S synthesis capability in the ischemic brain tissue. The results revealed that, compared to the sham group at corresponding time points, the model group demonstrated significant upregulation of CBS and SHH proteins ($p < 0.05$), with higher levels of CBS protein expression observed in the model-7d group than the model-14d group ($p < 0.05$). Compared to those of the sham and model groups, the GYY4137-treated group exhibited a significant reduction in the CBS protein expression (both $p < 0.05$) and a marked elevation in the SHH protein expression (both $p < 0.05$) (Fig. 11).

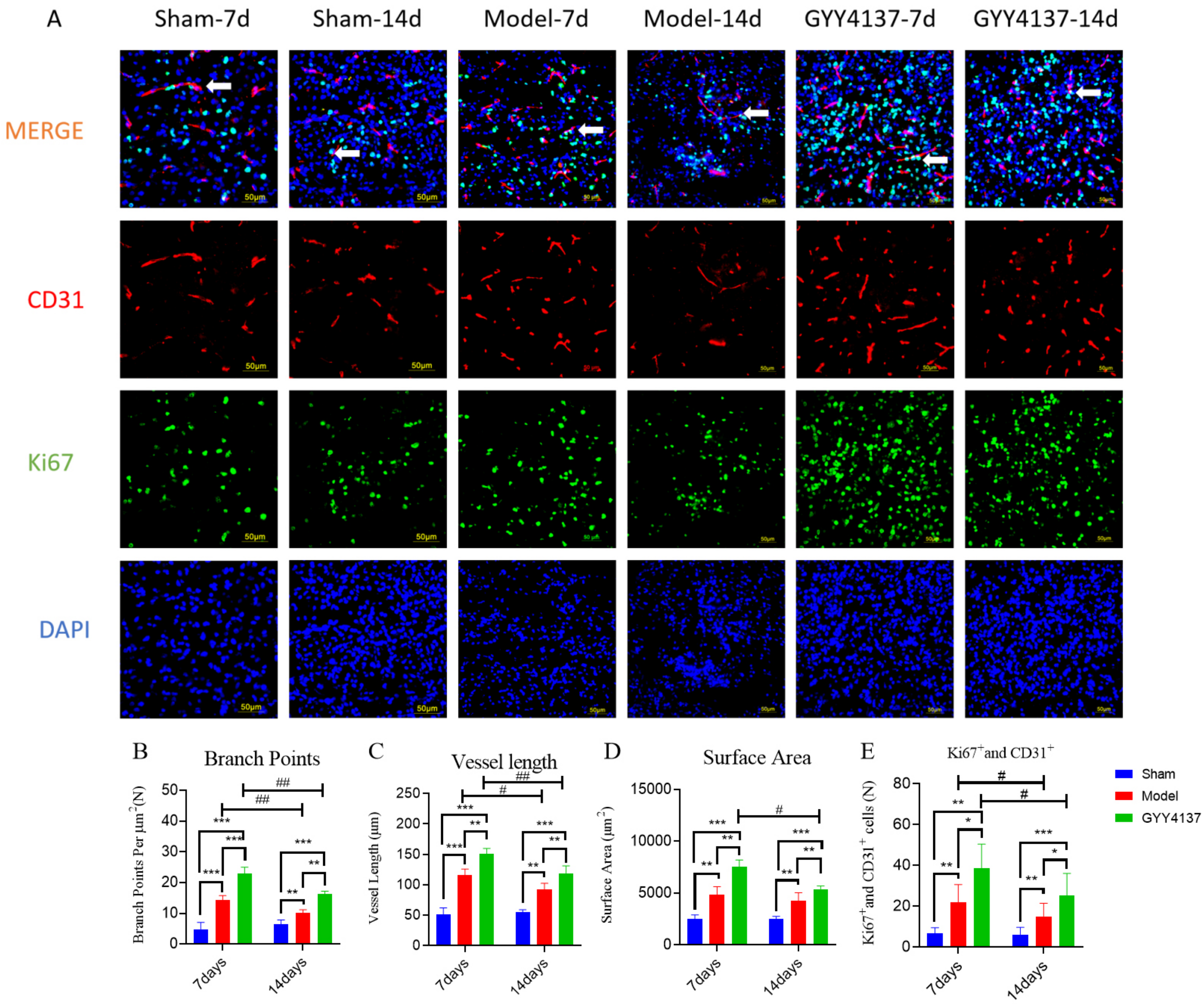

Fig. 6. H_2S enhanced angiogenesis indicated by stimulation of Ki67/CD31 co-localization. (A) Representative fluorescent micrographs of $CD31^+/Ki67^+$ co-staining. White arrows indicate $Ki67^+/CD31^+$ double-positive cells. (B–E) Quantitative analysis of neovascular branch point number, vessel length, surface area, and the number of $CD31^+/Ki67^+$ double-positive cells that represent the proliferating endothelial cells. Notes: $^*p < 0.05$, $^{**}p < 0.01$, $^{***}p < 0.001$, $^{\#}p < 0.05$, $^{\#\#}p < 0.01$; each group consisted of 6 rats (n = 6). Magnification: 400×, Scale bar: 50 µm.

Discussion

In this study, GYY4137 was incorporated into the experiments as the H_2S donor to investigate the modulatory relationship between H_2S and the SHH signaling pathway. Additionally, it investigated the role of H_2S in regulating angiogenesis following cerebral ischemia-reperfusion injury in rats through the SHH signaling pathway, and delineated its underlying mechanisms. By measuring plasma H_2S levels in rats before model establishment, as well as at 7- and 14-day post-modeling, we observed that relative to the sham-operated cohort, the model cohort presented with a marked increase in H_2S levels, which decreased notably over time. The trend in the H_2S levels was consistent with those of the neurological impairment and the infarct volume in the rats, indicating a close correlation between H_2S levels and symptoms of ischemic stroke in rats. Previous research has shown that H_2S can alleviate infarct volume in rats with ischemic stroke [18], suppress inflammatory responses by activating the AMP-activated protein kinase pathway through the supplementation of exogenous H_2S donors [19], and reduce the extent of infarct damage [20]. To further verify the relationship between H_2S levels and ischemic stroke in rats, this study treated MCAO/R rats with GYY4137, a slow-releasing H_2S donor. Comparative evaluations revealed that, in contrast to the model group, the GYY4137-treated group showed significantly increased H_2S levels, along with marked improvements in body weight, neurological deficit symptoms, infarct volume, and pathological damage; this was particularly evident

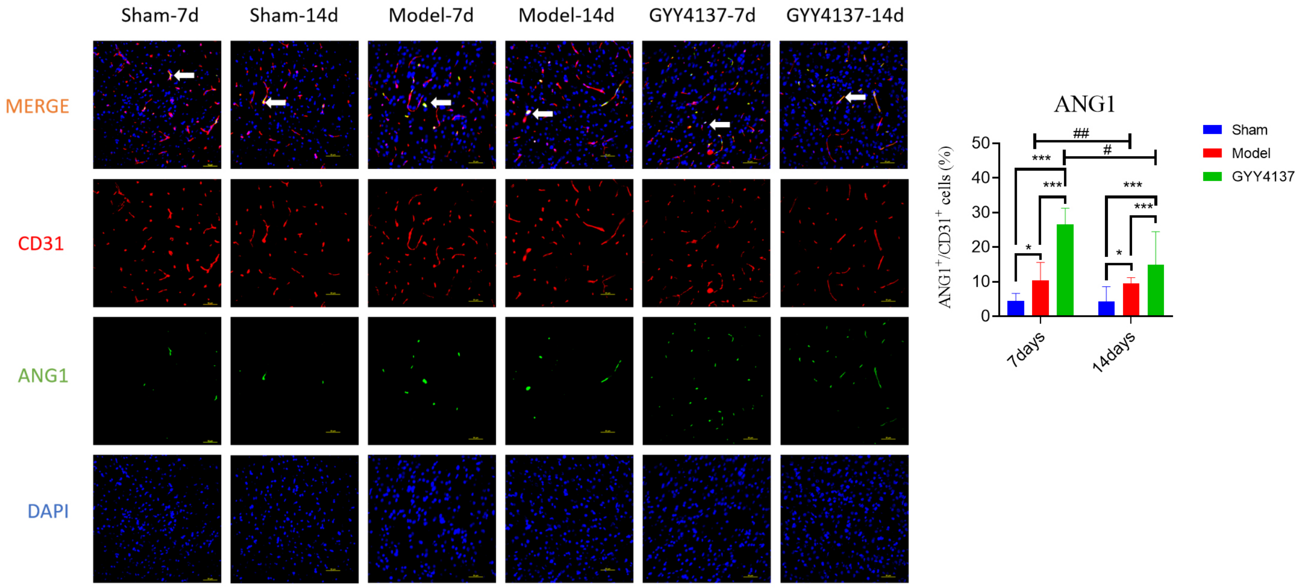

Fig. 7. GYY4137 enhances angiopoietin 1 (ANG1) expression in the peri-infarct cortex of MCAO/R rats. The y-axis in the bar chart represents the percentage of ANG1 expression relative to CD31 expression, as an indication of co-localization ratio. White arrows indicate ANG1$^+$/CD31$^+$ double-positive cells. Notes: $^{*}p < 0.05$, $^{***}p < 0.001$; $^{\#}p < 0.05$, $^{\#\#}p < 0.01$; each group had 6 rats (n = 6). Magnification: 400×; Scale bar: 50 µm.

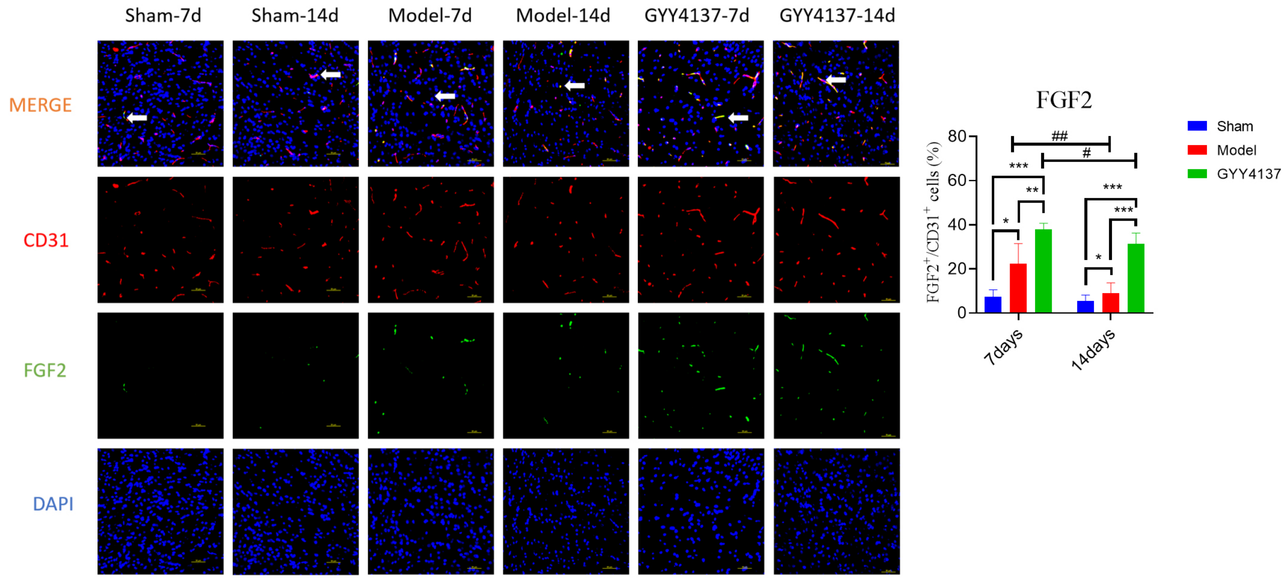

Fig. 8. H_2S upregulates FGF2 expression in the peri-infarct cortex of MCAO/R rats. The y-axis in the bar chart represents the percentage of FGF2 expression relative to CD31 expression, as an indication of co-localization ratio. White arrows indicate FGF2$^+$/CD31$^+$ double-positive cells. Notes: $^{*}p < 0.05$, $^{**}p < 0.01$, $^{***}p < 0.001$; $^{\#}p < 0.05$, $^{\#\#}p < 0.01$; each group consisted of 6 rats (n = 6). Magnification: 400×; Scale bar: 50 µm.

in the early stages. These findings suggest that H_2S can alleviate neurological impairment in rats, consistent with results of multiple previous studies [21–23]. Additionally, our study demonstrated that the GYY4137 restored CBF in rats following ischemia-reperfusion injury, indicating that H_2S may mitigate neurological impairment by improving CBF in rats.

It has been reported that H_2S plays a crucial regulatory role in angiogenesis. Specifically, at certain concentration, H_2S can promote proliferation, migration, and adhesion of endothelial cells, thereby promoting the formation of microvessels and improving tissue ischemia [24,25]. The results of this study revealed that H_2S increases CBF, improves neurological deficit symptoms, and reduces in-

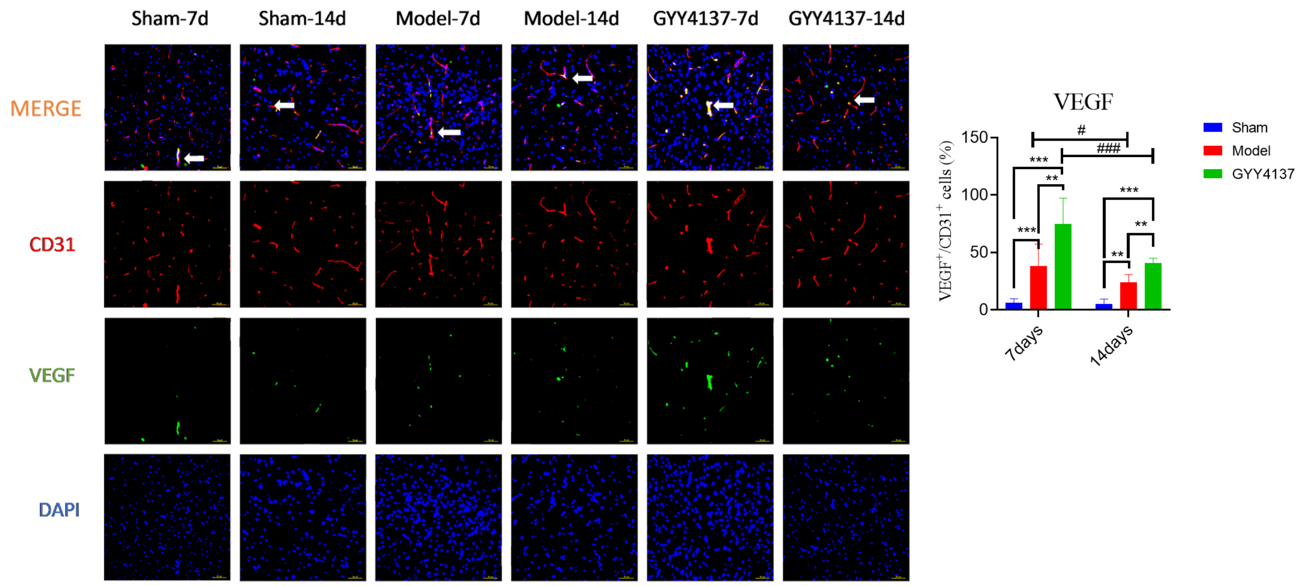

Fig. 9. GYY4137 enhances VEGF expression in the peri-infarct cortex of MCAO/R rats. The y-axis in the bar chart represents the percentage of VEGF expression relative to CD31 expression, as an indication of co-localization ratio. White arrows indicate VEGF$^+$/CD31$^+$ double-positive cells. Notes: $^{**}p < 0.01$, $^{***}p < 0.001$; $^{\#}p < 0.05$, $^{\#\#\#}p < 0.001$; each group consisted of 6 rats ($n = 6$). Magnification: 400×; Scale bar: 50 µm.

farct volume of the MCAO/R rats. To investigate whether this effect is attributable to the promotion of angiogenesis, we used Ki67 and CD31 co-staining to detect the density of new blood vessels in the peri-infarct cortical tissues of the MCAO/R rats. The results showed that ischemia-reperfusion injury induced angiogenesis, which was enhanced by H_2S. Angiogenesis is a critical therapeutic target with significant clinical potential for promoting recovery from ischemic pathologies. Emerging evidence supports the efficacy of H_2S as a cardioprotective modulator, which maintains cardiovascular homeostasis through multi-faceted mechanisms by achieving vasodilation, neovascularization, inflammatory regulation, redox balance, and apoptotic control [26]. In hypoxic microenvironments, H_2S stimulates endothelial cell growth and motility while enhancing angiogenic responses via upregulated VEGF expression. Furthermore, H_2S exerts pro-angiogenic effects through suppression of mitochondrial electron transfer and oxidative phosphorylation, resulting in elevated glucose utilization and glycolytic ATP synthesis [27]. Consistent with our findings, a report has shown that exogenous H_2S can significantly increase vascular density at the infarct border zone in rats with myocardial infarction [28], suggesting that H_2S may regulate neurological function through angiogenesis. This pro-angiogenic effect may be related to the activation of multiple angiogenic factors and their downstream signaling pathways by H_2S. VEGF and its downstream signaling pathways are closely related. VEGF represents a critical growth factor characterized by potent angiogenic properties. It stimulates endothelial cell division and survival, enhances vascular permeability, and facilitates cellular motility, thereby regulating physiological and pathological processes of neovascularization [29]. FGF modulates diverse physiological processes, encompassing embryonic development, vascular formation, tissue regeneration, homeostatic maintenance, and oncogenic progression. This growth factor regulates cellular proliferation, lineage specification, migratory capacity, viability, and metabolic activity in target cell populations [30]. ANG1 plays a pivotal role in vascular maturation, mediating the migration, adhesion, and survival of endothelial cells [31]. VEGF, FGF2, and ANG1 are inducers of angiogenesis. Evidence suggests that H_2S promotes collateral vessel growth and enhances local tissue perfusion in rats with unilateral hindlimb ischemia by upregulating VEGF and its downstream signaling effector, AKT, in skeletal muscle cells [32]. H_2S alleviates brain injury caused by deep hypothermic circulatory arrest through FGF2 [33]. In ischemic cerebrovascular conditions, H_2S exerts a neuroprotective effect by activating AKT/ERK phosphorylation cascades and upregulating VEGF/ANG1 protein expression [34]. This dual action promotes angiogenesis and cellular survival, alleviating ischemic damage. The synergistic modulation of these pathways highlights H_2S's therapeutic potential in cerebrovascular disease. To explore the mechanism behind H_2S regulation of angiogenesis in MCAO/R rats, we used double immunofluorescence staining to quantify the concentrations of ANG1, FGF2, and VEGF proteins in the peri-infarct cortical tissues of the rats. The results showed that GYY4137 intervention upregulated the expression of ANG1, FGF2, and VEGF proteins, suggesting that H_2S can enhance the expression of these proteins

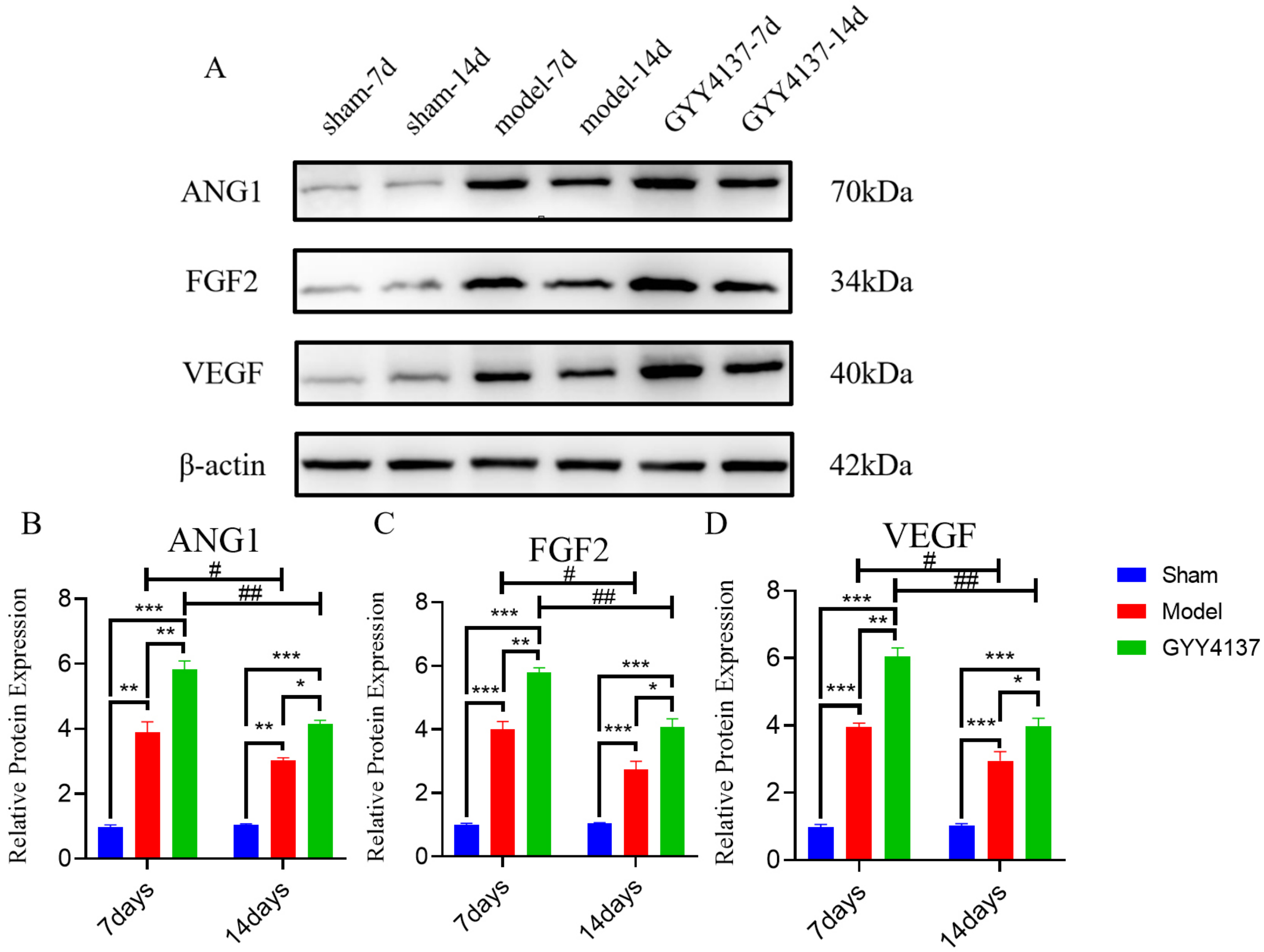

Fig. 10. ANG1, FGF2 and VEGF protein expression in the peri-infarct cortex of MCAO/R rats. (A) Western blot of the ANG1, FGF2 and VEGF proteins. (B–D) Quantitative analysis of protein expression of ANG1, FGF2 and VEGF across all treatment groups. Notes: $^{*}p < 0.05$, $^{**}p < 0.01$, $^{***}p < 0.001$; $^{\#}p < 0.05$, $^{\#\#}p < 0.01$; each group consisted of 6 rats (n = 6).

in the peri-infarct cortical tissues of MCAO/R rats, thereby promoting angiogenesis, with more pronounced effects in the early stage. The results of this study indicated that H_2S may regulate angiogenesis through the expression of angiogenesis-related factors.

The SHH signaling pathway plays a critical role in the development of the central nervous system in vertebrates, participating in neuronal patterning, cell fate specification, axonal guidance, proliferation, survival, and differentiation [35]. A study has shown that blocking the SHH signaling pathway in rodent models, following localized brain ischemia, exacerbates ischemic myelin injury [36]. Elevated SHH levels have been detected in the serum of patients with acute ischemic stroke and in the serum, cerebrospinal fluid, and ischemic brain tissues of MCAO/R rodent models. Reduction of SHH expression suppresses fibrotic scar development and M2 microglial activation in MCAO/R rodents, concurrently exacerbating neurological impairment [37]. The results of this study revealed that SHH expression increases after ischemia-reperfusion injury, consistent with the results of previous reports. Additionally, this study demonstrated that the GYY4137 intervention upregulated SHH expression, indicating the potential role of H_2S in regulating neurological recovery in ischemic stroke by mediating the SHH signaling pathway. Furthermore, evidence shows that the SHH signaling pathway regulates injury-induced angiogenesis and that inhibition of the SHH signaling pathway leads to decreased VEGF expression [38]. During ischemic stroke, the SHH increases the expression of ANG1 in the ischemic penumbra, promoting angiogenesis and vascular maturation [39]. The SHH signaling pathway also enhances ERK expression and phosphorylation, promoting cell proliferation and migration [40]. It has also been reported that active ingredients from *Trillium tschonoskii* can protect against cognitive impairment in post-stroke rats by inhibiting apoptosis and enhancing neuronal synaptic plasticity via SHH signaling [41]. These findings highlight the potential association between H_2S treatment and SHH signaling pathway activation in promoting angiogenesis, which may contribute

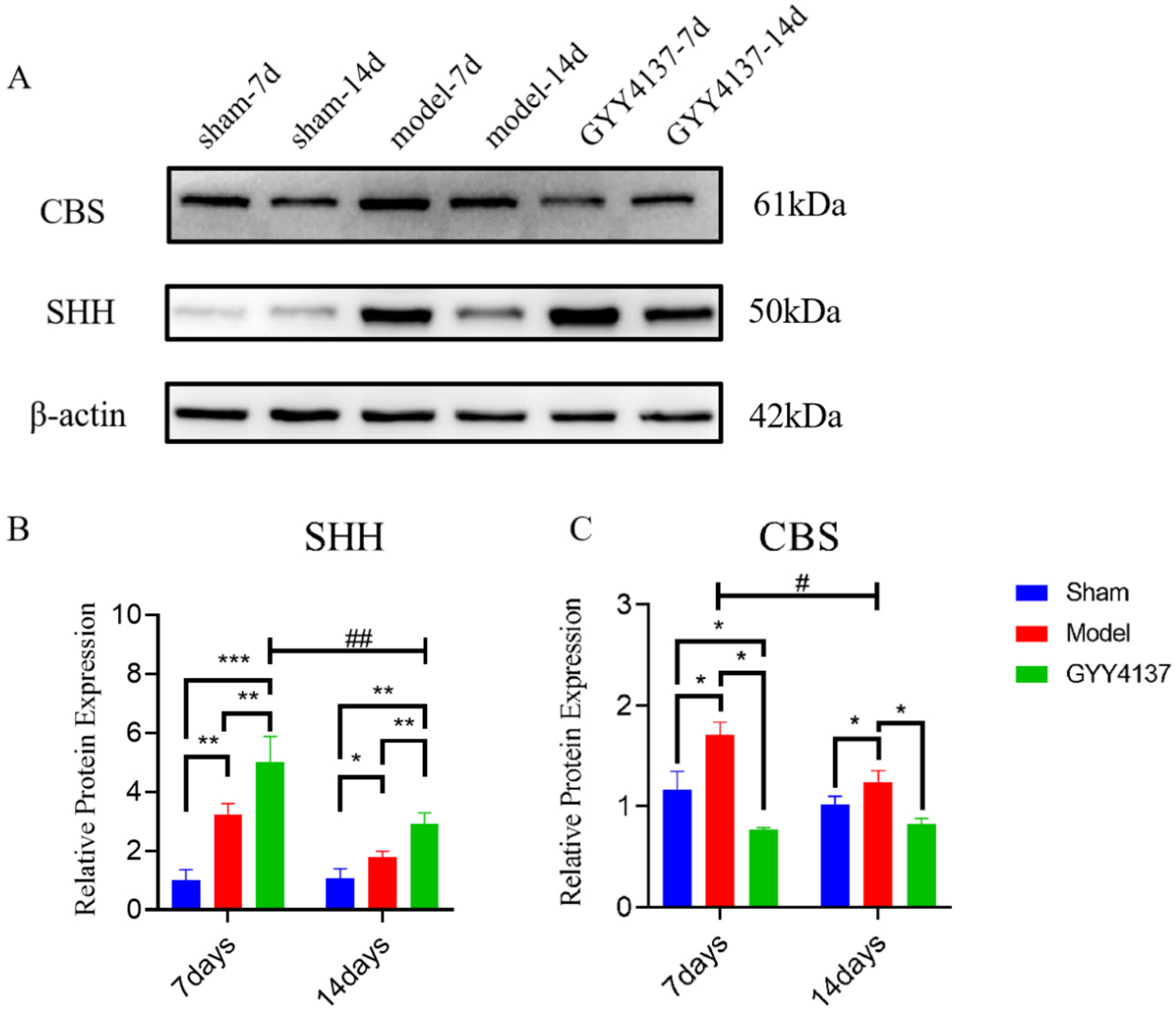

Fig. 11. H_2S upregulates Sonic hedgehog (SHH) and downregulates cystathionine-β-synthase (CBS) protein expression in the peri-infarct cortex of MCAO/R rats. (A) Western blot of the SHH and CBS proteins. (B,C) Quantitative analysis of protein expression of SHH and CBS across allgroups. Notes: $^{*}p < 0.05$, $^{**}p < 0.01$, $^{***}p < 0.001$; $^{\#}p < 0.05$, $^{\#\#}p < 0.01$; each group consisted of six rats (n = 6).

to preserved CBF and improved neurological function in MCAO/R rats. However, whether H_2S directly regulates angiogenesis through the SHH pathway requires further mechanistic validation using pathway-specific inhibitors or genetic manipulation approaches.

Angiogenesis after ischemic stroke is critical for restoring blood flow and neurological function. As a novel gaseous signaling molecule, H_2S plays multiple beneficial roles in angiogenesis. Despite evidence regarding the protective effects of H_2S in ischemic stroke, the current *in vitro* and animal experiments on H_2S remain in the experimental stage and application of this agent has yet to be translated into clinical settings. The results of this study demonstrate that H_2S promotes the upregulation of multiple pro-angiogenic factors such as VEGF, FGF2 and ANG1 via the SHH signaling pathway, contributing to the angiogenic process following cerebral ischemia. The induction of angiogenesis facilitates the establishment of collateral circulation, which in turn improves the neurological deficits caused by cerebral ischemia. Our findings in this study support the therapeutic and rehabilitative potential of H_2S following ischemic stroke, positioning it as a promising intervention agent in the future.

Conclusion

In conclusion, exogenous H_2S delivered via the GYY4137 intervention promotes angiogenesis in the ischemic penumbra of MCAO/R rats by upregulating VEGF, ANG1, and FGF2 expression, which is accompanied by activation of the SHH signaling pathway. Our findings suggest a potential mechanistic link between H_2S treatment and SHH pathway activation in promoting post-stroke angiogenesis, although direct causality requires further validation through pathway inhibition or genetic manipulation studies.

Abbreviations

H_2S, hydrogen sulfide; SHH, Sonic hedgehog; CBS, cystathionine-β-synthase; VEGF, vascular endothelial growth factor; FGF2, fibroblast growth factor 2; ANG1, angiopoietin 1; MCAO/R, middle cerebral artery occlusion/reperfusion; CBF, cerebral blood flow.

Availability of Data and Materials

The datasets generated and/or analyzed during the current study are not publicly available, but are available from the corresponding authors (Jianmin Huang and Xuebin Li) on reasonable request.

Author Contributions

Conception and design of the study: HC, XL, JH, JW; Acquisition of data: PZ, GY, BQ, TW; Analysis and interpretation of the data: BQ, PZ, GY; Statistical analysis: JW, BQ, TW; Obtaining financing: XL, HC; Writing of the manuscript: HC, XL, BQ, JW; Critical revision of the manuscript for intellectual content: all authors. All authors read and approved the final draft. All authors have participated sufficiently in the work and agreed to be accountable for all aspects of the work.

Ethics Approval and Consent to Participate

All animal procedures were approved by the Ethics Committee of Youjiang Medical University for Nationalities (Approval No. 2023102701) and carried out in accordance with the guidelines for the care and use of laboratory animals.

Acknowledgment

Not applicable.

Funding

This study was supported by a grant from National Natural Science Foundation of China (No. 81860226), Guangxi Medical and Health Appropriate Technology Development and Application Project (No. S2018073), Young and Middle-aged Backbone Talent Scientific Research Projects of the Affiliated Hospital of Youjiang Medical University for Nationalities in 2021 (No. Y20212610), and Guangxi Health Commission Self -Financed Research Project (No. Z-L20230898).

Conflict of Interest

The authors declare no conflict of interest.

References

[1] Anadani M, Finitsis S, Clarençon F, Richard S, Marnat G, Bourcier R, *et al*. Collateral status reperfusion and outcomes after endovascular therapy: insight from the Endovascular Treatment in Ischemic Stroke (ETIS) Registry. Journal of Neurointerventional Surgery. 2022; 14: 551–557. https://doi.org/10.1136/neurintsurg-2021-017553.

[2] Binder NF, El Amki M, Glück C, Middleham W, Reuss AM, Bertolo A, *et al*. Leptomeningeal collaterals regulate reperfusion in ischemic stroke and rescue the brain from futile recanalization. Neuron. 2024; 112: 1456–1472.e6. https://doi.org/10.1016/j.neuron.2024.01.031.

[3] Wang Y, Shan Y, Lu J. Research progress of multimodal CT in evaluating collateral circulation of ischemic stroke. Chinese Journal of Geriatric Heart Brain and Vessel Diseases. 2022; 24: 1006–1008. (In Chinese)

[4] Huang J, Li X, Zhao J, Chen H, Yun Y, Yang G, *et al*. Association of BIRC5 Gene Polymorphism with the Collateral Circulation and Severity of Large Artery Atherosclerotic Stroke. International Journal of Clinical Practice. 2022; 2022: 9177545. https://doi.org/10.1155/2022/9177545.

[5] Zhang P, Yu Y, Wang P, Shen H, Ling X, Xue X, *et al*. Role of Hydrogen Sulfide in Myocardial Ischemia-Reperfusion Injury. Journal of Cardiovascular Pharmacology. 2021; 77: 130–141. https://doi.org/10.1097/FJC.0000000000000943.

[6] Zhang YX, Jing MR, Cai CB, Zhu SG, Zhang CJ, Wang QM, *et al*. Role of hydrogen sulphide in physiological and pathological angiogenesis. Cell Proliferation. 2023; 56: e13374. https://doi.org/10.1111/cpr.13374.

[7] Pietrobono S, Gagliardi S, Stecca B. Non-canonical Hedgehog Signaling Pathway in Cancer: Activation of GLI Transcription Factors Beyond Smoothened. Frontiers in Genetics. 2019; 10: 556. https://doi.org/10.3389/fgene.2019.00556.

[8] Sigafoos AN, Paradise BD, Fernandez-Zapico ME. Hedgehog/GLI Signaling Pathway: Transduction, Regulation, and Implications for Disease. Cancers. 2021; 13: 3410. https://doi.org/10.3390/cancers13143410.

[9] Lee SW, Moskowitz MA, Sims JR. Sonic hedgehog inversely regulates the expression of angiopoietin-1 and angiopoietin-2 in fibroblasts. International Journal of Molecular Medicine. 2007; 19: 445–451.

[10] Fujii T, Kuwano H. Regulation of the expression balance of angiopoietin-1 and angiopoietin-2 by Shh and FGF-2. In Vitro Cellular & Developmental Biology. Animal. 2010; 46: 487–491. https://doi.org/10.1007/s11626-009-9270-x.

[11] Lawson ND, Vogel AM, Weinstein BM. sonic hedgehog and vascular endothelial growth factor act upstream of the Notch pathway during arterial endothelial differentiation. Developmental Cell. 2002; 3: 127–136. https://doi.org/10.1016/s1534-5807(02)00198-3.

[12] Xu Y, Ma N, Wei P, Zeng Z, Meng J. Expression of hydrogen sulfide synthases and Hh signaling pathway components correlate with the clinicopathological characteristics of papillary thyroid cancer patients. International Journal of Clinical and Experimental Pathology. 2018; 11: 1818–1824.

[13] Hu X, Xiao Y, Sun J, Ji B, Luo S, Wu B, *et al*. New possible silver lining for pancreatic cancer therapy: Hydrogen sulfide and its donors. Acta Pharmaceutica Sinica. B. 2021; 11: 1148–1157. https://doi.org/10.1016/j.apsb.2020.10.019.

[14] Min Z, Li C, Fang Y, Qiu Z, Zhang Su. Application of laser

speckle imaging technique in observing collateral circulation in a rat middle cerebral artery occlusion model. Neural Injury and Functional Reconstruction. 2014; 191–194. (In Chinese)
[15] Longa EZ, Weinstein PR, Carlson S, Cummins R. Reversible middle cerebral artery occlusion without craniectomy in rats. Stroke. 1989; 20: 84–91. https://doi.org/10.1161/01.str.20.1.84.
[16] Schaar KL, Brenneman MM, Savitz SI. Functional assessments in the rodent stroke model. Experimental & Translational Stroke Medicine. 2010; 2: 13. https://doi.org/10.1186/2040-7378-2-13.
[17] Song Q, Che Z, Zou Y. Selection of blood collection methods for laboratory rats. Chinese Journal of Tissue Engineering Research and Clinical Rehabilitation. 2008; 12: 9990–9992. (In Chinese)
[18] Woo CW, Kwon JI, Kim KW, Kim JK, Jeon SB, Jung SC, *et al*. The administration of hydrogen sulphide prior to ischemic reperfusion has neuroprotective effects in an acute stroke model. PloS One. 2017; 12: e0187910. https://doi.org/10.1371/journal.pone.0187910.
[19] Chu X, Cao L, Yu Z, Xin D, Li T, Ma W, *et al*. Hydrogen-rich saline promotes microglia M2 polarization and complement-mediated synapse loss to restore behavioral deficits following hypoxia-ischemic in neonatal mice via AMPK activation. Journal of Neuroinflammation. 2019; 16: 104. https://doi.org/10.1186/s12974-019-1488-2.
[20] Zhang M, Wu X, Xu Y, He M, Yang J, Li J, *et al*. The cystathionine β-synthase/hydrogen sulfide pathway contributes to microglia-mediated neuroinflammation following cerebral ischemia. Brain, Behavior, and Immunity. 2017; 66: 332–346. https://doi.org/10.1016/j.bbi.2017.07.156.
[21] Han X, Mao Z, Wang S, Xin Y, Li P, Maharjan S, *et al*. GYY4137 protects against MCAO via p38 MAPK mediated anti-apoptotic signaling pathways in rats. Brain Research Bulletin. 2020; 158: 59–65. https://doi.org/10.1016/j.brainresbull.2020.02.015.
[22] Song YJ, Shi Y, Cui MM, Li M, Wen XR, Zhou XY, *et al*. H2S attenuates injury after ischemic stroke by diminishing the assembly of CaMKII with ASK1-MKK3-p38 signaling module. Behavioural Brain Research. 2020; 384: 112520. https://doi.org/10.1016/j.bbr.2020.112520.
[23] Ren C, Du A, Li D, Sui J, Mayhan WG, Zhao H. Dynamic change of hydrogen sulfide during global cerebral ischemia-reperfusion and its effect in rats. Brain Research. 2010; 1345: 197–205. https://doi.org/10.1016/j.brainres.2010.05.017.
[24] Wang MJ, Cai WJ, Li N, Ding YJ, Chen Y, Zhu YC. The hydrogen sulfide donor NaHS promotes angiogenesis in a rat model of hind limb ischemia. Antioxidants & Redox Signaling. 2010; 12: 1065–1077. https://doi.org/10.1089/ars.2009.2945.
[25] Xi H, Wang C, Li Q, Ye Q, Zhu Y, Mao Y. S-Propargyl-Cysteine Ameliorates Peripheral Nerve Injury through Microvascular Reconstruction. Antioxidants (Basel, Switzerland). 2023; 12: 294. https://doi.org/10.3390/antiox12020294.
[26] Wang YZ, Ngowi EE, Wang D, Qi HW, Jing MR, Zhang YX, *et al*. The Potential of Hydrogen Sulfide Donors in Treating Cardiovascular Diseases. International Journal of Molecular Sciences. 2021; 22: 2194. https://doi.org/10.3390/ijms22042194.
[27] Wang RH, Chen PR, Chen YT, Chen YC, Chu YH, Chien CC, *et al*. Hydrogen sulfide coordinates glucose metabolism switch through destabilizing tetrameric pyruvate kinase M2. Nature Communications. 2024; 15: 7463. https://doi.org/10.1038/s41467-024-51875-9.
[28] Łoboda A, Dulak J. Cardioprotective Effects of Hydrogen Sulfide and Its Potential Therapeutic Implications in the Amelioration of Duchenne Muscular Dystrophy Cardiomyopathy. Cells. 2024; 13: 158. https://doi.org/10.3390/cells13020158.
[29] Melincovici CS, Boşca AB, Şuşman S, Mărginean M, Mihu C, Istrate M, *et al*. Vascular endothelial growth factor (VEGF) - key factor in normal and pathological angiogenesis. Romanian Journal of Morphology and Embryology = Revue Roumaine De Morphologie et Embryologie. 2018; 59: 455–467.
[30] Yang L, Zhou F, Zheng D, Wang D, Li X, Zhao C, *et al*. FGF/FGFR signaling: From lung development to respiratory diseases. Cytokine & Growth Factor Reviews. 2021; 62: 94–104. https://doi.org/10.1016/j.cytogfr.2021.09.002.
[31] Sha L, Zhao Y, Li S, Wei D, Tao Y, Wang Y. Insights to Ang/Tie signaling pathway: another rosy dawn for treating retinal and choroidal vascular diseases. Journal of Translational Medicine. 2024; 22: 898. https://doi.org/10.1186/s12967-024-05441-y.
[32] Yang H, Tan M, Gao Z, Wang S, Lyu L, Ding H. Role of Hydrogen Sulfide and Hypoxia in Hepatic Angiogenesis of Portal Hypertension. Journal of Clinical and Translational Hepatology. 2023; 11: 675–681. https://doi.org/10.14218/JCTH.2022.00217.
[33] Zhu YX, Yang Q, Zhang YP, Liu ZG. FGF2 Functions in H_2S's Attenuating Effect on Brain Injury Induced by Deep Hypothermic Circulatory Arrest in Rats. Molecular Biotechnology. 2024; 66: 3526–3537. https://doi.org/10.1007/s12033-023-00952-3.
[34] Wu D, Zhong P, Wang Y, Zhang Q, Li J, Liu Z, *et al*. Hydrogen Sulfide Attenuates High-Fat Diet-Induced Non-Alcoholic Fatty Liver Disease by Inhibiting Apoptosis and Promoting Autophagy via Reactive Oxygen Species/Phosphatidylinositol 3-Kinase/AKT/Mammalian Target of Rapamycin Signaling Pathway. Frontiers in Pharmacology. 2020; 11: 585860. https://doi.org/10.3389/fphar.2020.585860.
[35] Prajapati A, Mehan S, Khan Z. The role of Smo-Shh/Gli signaling activation in the prevention of neurological and ageing disorders. Biogerontology. 2023; 24: 493–531. https://doi.org/10.1007/s10522-023-10034-1.
[36] Zhao H, Gao XY, Wu XJ, Zhang YB, Wang XF. The Shh/Gli1 signaling pathway regulates regeneration via transcription factor Olig1 expression after focal cerebral ischemia in rats. Neurological Research. 2022; 44: 318–330. https://doi.org/10.1080/01616412.2021.1981106.
[37] Yang Q, Jiang P, Tang H, Wen J, Zhou L, Zhao Y, *et al*. Shh regulates M2 microglial polarization and fibrotic scar formation after ischemic stroke. Neurochemistry International. 2024; 180: 105862. https://doi.org/10.1016/j.neuint.2024.105862.
[38] Straface G, Aprahamian T, Flex A, Gaetani E, Biscetti F, Smith RC, *et al*. Sonic hedgehog regulates angiogenesis and myogenesis during post-natal skeletal muscle regeneration. Journal of Cellular and Molecular Medicine. 2009; 13: 2424–2435. https://doi.org/10.1111/j.1582-4934.2008.00440.x.
[39] Xia YP, He QW, Li YN, Chen SC, Huang M, Wang Y, *et al*. Recombinant human sonic hedgehog protein regulates the expression of ZO-1 and occludin by activating angiopoietin-1 in stroke damage. PloS One. 2013; 8: e68891. https://doi.org/10.1371/journal.pone.0068891.
[40] Liu F, Feng XX, Zhu SL, Huang HY, Chen YD, Pan YF, *et al*. Sonic Hedgehog Signaling Pathway Mediates Proliferation and Migration of Fibroblast-Like Synoviocytes in Rheumatoid Arthritis *via* MAPK/ERK Signaling Pathway. Frontiers in Immunology. 2018; 9: 2847. https://doi.org/10.3389/fimmu.2018.02847.
[41] Wang G, Tang X, Zhao F, Qin X, Wang F, Yang D, *et al*. Total saponins from *Trillium tschonoskii* Maxim promote neurological recovery in model rats with post-stroke cognitive impairment. Frontiers in Pharmacology. 2023; 14: 1255560. https://doi.org/10.3389/fphar.2023.1255560.